DEVELOPMENTAL ASSESSMENT OF IFCI 6.0
ASME

DEVELOPMENTAL ASSESSMENT OF IFCI 6.0*

Alfred W. Reed, Michael F. Young, and Rodney C. Schmidt
Nuclear Energy Technology Center
Sandia National Laboratories
Albuquerque, New Mexico

ABSTRACT

Version 6.0 of the IFCI code is being assessed by comparing predictions against the results of several experiments. Simulations of the first two of these experiments, MAGICO-701 and MIXA-6, have been completed with a reasonable level of success. Agreement with the MAGICO-701 experiment was good but was limited somewhat by the inherent problem of numerical diffusion. Results of the MIXA-6 calculations were comparable to those of CHYMES, but clearly suggested the need for an inter-cell radiation transport model in IFCI.

INTRODUCTION

The Integrated Fuel-Coolant Interaction (IFCI) code is designed to model the mixing of molten nuclear reactor materials with reactor coolant (water). (Young, 1991; Davis and Young, 1994) It is designed to handle, with varying degrees of empiricism, the four stages of fuel-coolant interactions: coarse mixing, triggering, detonation propagation, and hydrodynamic expansion. IFCI contains models for boiling rates, flow regimes, dynamic melt fragmentation, surface tracking, subcooling effects, melt oxidation, triggering, and propagation of the shock. These phenomena are essential to the modeling of fuel/coolant interactions. IFCI is under development at Sandia National Laboratories (SNL) and is sponsored by the United States Nuclear Regulatory Commission, Office of Nuclear Regulatory Research (USNRC/RES).

As part of the assessment of the current version of the code, calculations made by IFCI were compared to two experiments: MAGICO-701 and MIXA-6. These are the first two of a series of experiments against which IFCI was compared. The sequence of experiments was chosen to progress from the simple to the more complex. The MAGICO and MIXA experiments focused only on coarse mixing phenomena. The MAGICO experiments utilized hot stainless steel spheres heated to relatively low temperatures, and measured the steam volume fraction during mixing. These experiments provide a data base unaffected by particle breakup and thermal radiation. The MIXA experiments used molten urania at high temperature and measured the steam generation rate. The effects of melt fragmentation and thermal radiation, as well as small amounts of subcooling constituted the next level of complexity. Calculations are currently being conducted for the KROTOS experiments, which include the propagation phase of the FCI. Calculations are also planned to test the oxidation model within IFCI.

This document presents the results of the work conducted to date. Direct comparisons between experimental data and IFCI calculations are presented for the MAGICO-701 and MIXA-6 experiments. Additional modeling needs determined during the exercise are also presented.

MAGICO-701

Experiment Geometry and Results

The MAGICO experiments (Theofanous et. al., 1994) were designed to measure the vapor volume fraction in the region of the melt without the complicating phenomenon of particle breakup. This was accomplished by dropping hot steel (SS316) spheres from a perforated plate into a pool of water at the saturation temperature. The water was contained in a rectangular vessel (406 mm square by 355 mm high) made of tempered glass. The progression of the hot spheres downward in the pool and the

* Work sponsored by the U.S. Nuclear Regulatory Commission, Office of Nuclear Regulatory Research

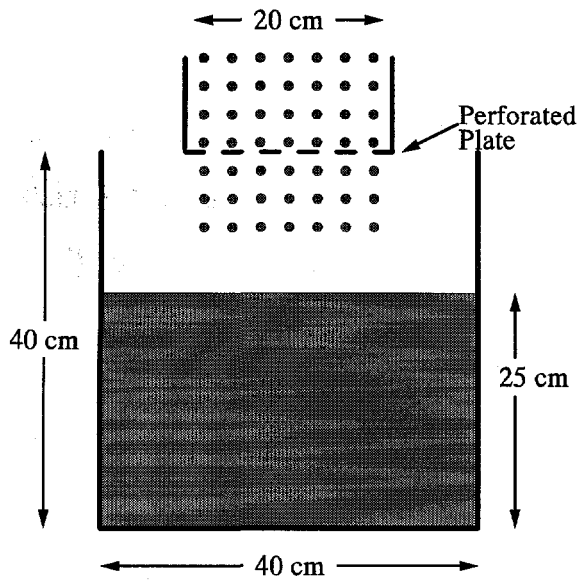

FIGURE 1 SCHEMATIC OF MAGICO-701 AS MODELED IN IFCI

resulting increase in the water level were recorded by video camera. The video indicated that there was little radial spreading of the boiling region. The average volume fraction in the mixing zone was deduced from the liquid swell and boiling front observed in the experiment video.

A number of combinations of initial water depths (h_0), sphere temperatures and diameters, and pour diameters (d_{pour}) defined the test series. The MAGICO 701 test had the parameters listed in

TABLE 1
MAGICO-701 EXPERIMENT PARAMETERS

Sphere Temperature	550 C
Sphere Diameter	2.4 mm
Pool Depth	25 cm
Freefall Distance	15 cm

TABLE 1. The sphere velocity immediately below the perforated plate was measured at 72 cm/second. The sphere volume fraction at the perforated plate was measured at 1.87%.

Comparison of IFCI Predictions with MAGICO-701 Measurements

The MAGICO-701 experiment domain was modeled as a right circular cylinder, having an outer radius of 20 cm. and a height of 40 cm. (FIGURE 1) In order to check for numerical diffusion, three mesh resolutions were used to model the MAGICO-701 experiment. The coarse, medium, and fine meshes contained 32, 64, and 104 axial cells, respectively. All of the

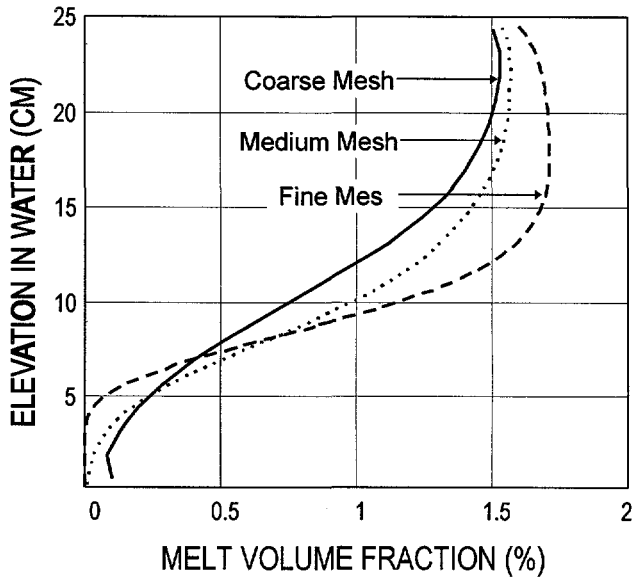

FIGURE 2 DISTRIBUTION OF PARTICULATE IN WATER AT CENTERLINE (0.23 SEC)

meshes contained 10 radial cells. The cell heights and radial lengths were uniform throughout the domain. The entry of steel spheres into the experiment was modeled by a mass flux condition at the top half of the domain. Steam was allowed to escape from the outer three cells at the top of the domain.

The predicted distribution of hot spheres in the water 0.23 seconds after initial entry is shown in FIGURE 2. The plot shows the predicted volume fraction of steel spheres at the centerline at 0.23 seconds after initial impact with the water surface. The volume fraction is approximately 1.5 % near the surface of the water. The volume fraction starts to decline at an elevation of about 15 cm to a value of about 0.35 % at an elevation of 7 cm.

The plot illustrates the differences in predictions between the coarse, medium, and fine meshes. The sphere front in the fine mesh has not touched the bottom while the sphere front in the medium mesh has just reached the bottom. The coarse mesh shows an accumulation of spheres on the bottom. The differences between the predictions are most likely due to numerical diffusion.

Sphere motion is not, in of itself, diffusive in nature. However, the use of an Eulerian (stationary) grid to model sphere motion adds an artificial diffusive component to the numerical solution for sphere motion. This results in the smeared leading edge that is evident in FIGURE 2. This means that a threshold volume fraction must be assigned in order to define the penetration front.

FIGURE 3 compares the measured front advancement with the IFCI predictions using a threshold volume fraction of 0.0005. The data shows a front that slows somewhat with increasing time. Although the data does not show the exact time of arrival of the front, extrapolation of the data suggests a transit time of

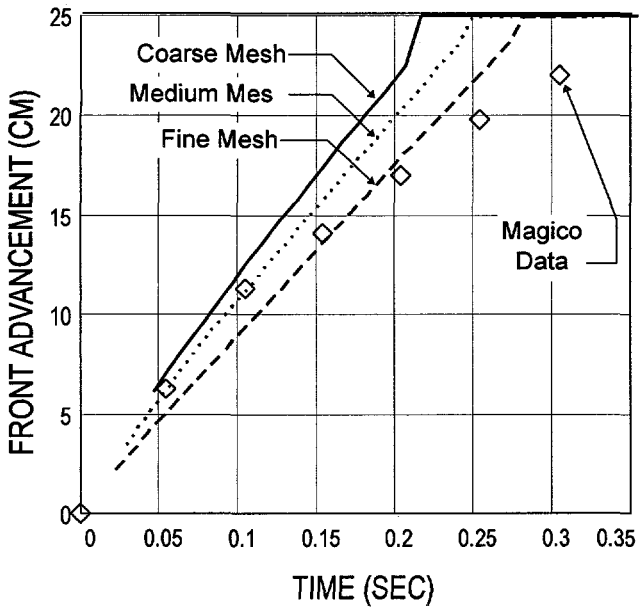

FIGURE 3 ADVANCEMENT OF THE FRONT OF HOT SPHERES (THRESHOLD=0.0005)

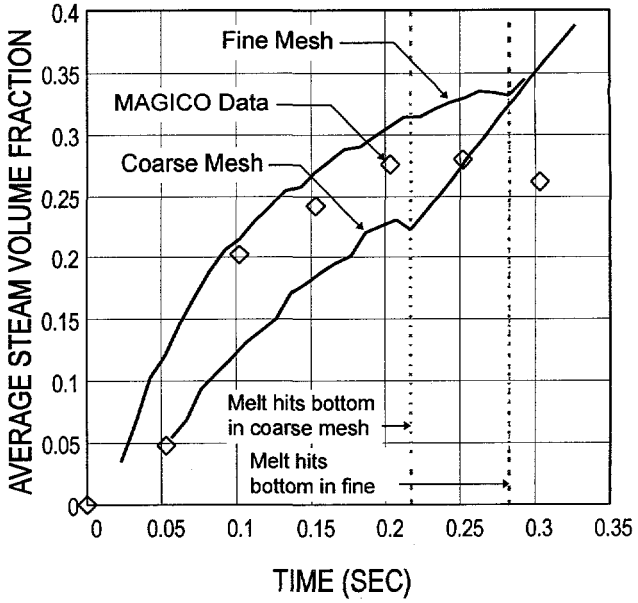

FIGURE 4 AVERAGE STEAM VOLUME FRACTION IN THE MELT REGION (THRESHOLD=0.0005)

approximately 0.35 seconds. IFCI predicts the location of the front accurately at early times, but does not exhibit the slowing of the front to the same degree as the data. The effect of meshing is evident in the predictions. The coarse, medium, and fine meshes show transit times of 0.22, 0.25, and 0.28 sec, respectively. Increasingly finer meshes improve the quality of the prediction.

The average vapor volume fraction in the region behind the advancing front is shown in FIGURE 4. The data shows an increase to approximately 0.28 % at about 0.2 sec, after which it remains approximately constant or declines somewhat. The IFCI predictions come reasonably close to the experimental data up through the calculated "melt" settling time. The coarse mesh underpredicts the data up until the predicted transit time of 0.22 seconds (shown as a vertical dotted line), after which the volume fraction increases linearly with time and eventually exceeds the data values. The fine mesh is much closer to the data over the predicted transit time of 0.28 seconds (shown as a second vertical dotted line). In the same manner as the coarse mesh, the predicted volume fraction increases linearly once the spheres arrive at the bottom of the experiment container. There is no experimental data for times after the spheres begin to touch the container bottom.

MIXA-6

Experiment Geometry

The MIXA experiments (Denham et. al., 1992; Fletcher and Denham, 1995) were designed to measure steam production rate during the coarse mixing stage of fuel/coolant interactions. A molten fuel simulant (81% UO_2, 19% Mo at 3600 K) was poured over a grid of carbon bars, which produced 16 streams of molten material. These streams broke up into droplets having a diameter of approximately 6 mm. A steel tube having an inside diameter of 122 mm was placed immediately below the carbon bars to constrain the lateral spreading of the melt. The length of the tube was varied between individual experiments. In the MIXA-6 experiment, the tube length was 480 mm. (FIGURE 5)

The molten material (3.0 kg for MIXA-6) was released into a pool of water from an elevation about 1 m. The water pool was square in cross section (0.37 m each side) with a depth of 0.6 m. The water was initially at saturation temperature at a pressure of 1 atmosphere. The volumetric steam flow rate was measured by a vortex flowmeter connected to the top of the experiment chamber

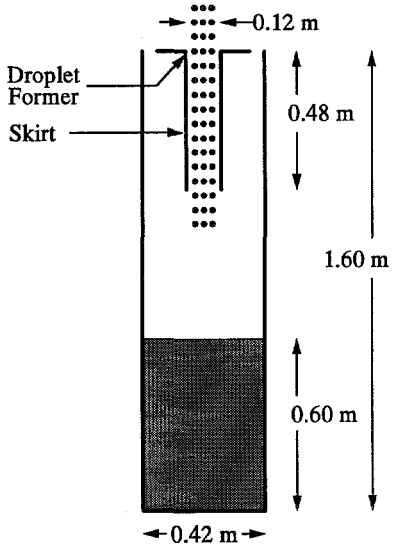

FIGURE 5 SCHEMATIC OF MIXA-6 AS MODELED IN IFCI

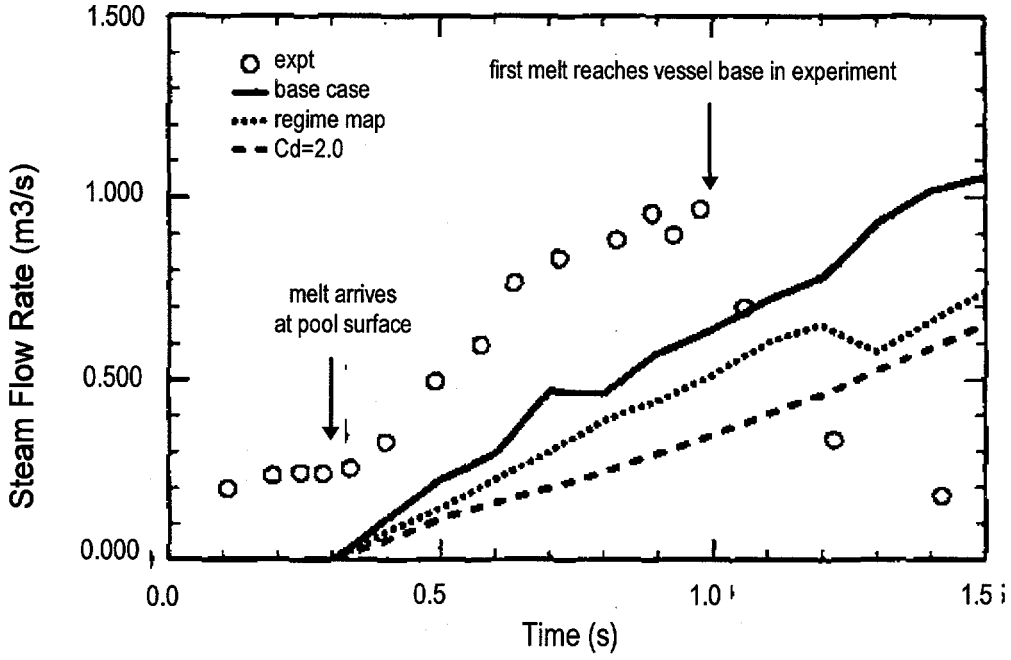

FIGURE 6 THE TRANSIENT STEAMING RATE: A COMPARISON OF THE CALCULATED VALUES WITH THE EXPERIMENTAL DATA (COPIED FROM FLETCHER AND DENHAM, 1995)

by a 100 mm diameter vent line (data shown in FIGURE 6). Pressure in the gas region of the chamber was measured using strain gauge pressure transducers (data shown in FIGURE 7).

Incorporation of Pressurization in IFCI

The MIXA-6 experiment displayed an increase in pressure from an initial value of 0.1 MPa to a peak pressure of 0.13 MPa. (FIGURE 7). This corresponds to an increase in the saturation temperature of approximately 7.5K. One can ignore the subcooling a priori only if the energy associated with subcooling is much less than the energy of the escaped steam. Based upon a water specific heat of 4.187 kJ/kg/-K and a water mass of 80 kg, there is a subcooling energy of about 2.5 MJ due to the increase in saturation temperature. The mass of steam generated by the experiment is obtained by integrating the product of the measured volume flow rate and the density as a function of saturation pressure. This integration produces a mass of 0.365 kg of steam that left the system between 0 and 1 second. Using an enthalpy of vaporization of 2.257 MJ/kg, the vaporization energy was 0.82 MJ. This is less than a third of the subcooling energy. This means that if the system were well stirred, the subcooling would be more than enough to condense all of the steam measured in the experiment. Although this does not guarantee that subcooling will affect the vapor generation rate, the possibility cannot be ruled out on the basis of first principles.

The IFCI code incorporates the effects of subcooling in its calculation of steam generation rate. It was therefore deemed necessary to include the pressurization of the test chamber in the calculation. This is done in IFCI by computing an effective flow area for the outflow boundary condition.

Order of magnitude estimates indicate that viscous drag on the walls of the vent tube was too small to explain the pressure drops measured in the MIXA-6 experiment. This means that the pressure drop is most likely due to kinetic losses at the entrance of the vent tube and at the throat in the vortex flowmeter. These types of pressure drops (ΔP) are usually modeled by the equation

$$\Delta P = K \rho_{steam} (\dot{Q}_{steam})^2 \quad ; K = \frac{k}{2A^2} \qquad (1)$$

where Q_{steam} is the volume flow rate of steam (m^3/sec), A is the flow area of the pipe or component (m^2), ρ_{steam} is the steam density (kg/m^3), and k is a loss coefficient (dimensionless) that is a function of the geometry. The value for K in this analysis is derived from the published data for the MIXA-6 experiment.

The steam volume flow rate (FIGURE 6) and the chamber pressure (FIGURE 7) for MIXA-6 were published as separate curves in Fletcher and Denham (1995). The curves, themselves, deserve some scrutiny. The time base for the pressure curve is the "time after the melt arrives at (the) water surface." The time on the volume flow rate curve is clearly the time after the melt is released. The time at which the melt hits the surface is clearly marked on this curve at about 0.32 seconds. If these time axes are correctly labeled, then the peak pressure occurred approximately 0.32 seconds after the steam flow rate peaked. This might be possible if water were transported into the flowmeter, choking the flow of steam in the meter throat. Another possibility is that the time axis of the pressure curve was mislabeled. If the time on the pressure curve were the time after the melt was released, then the

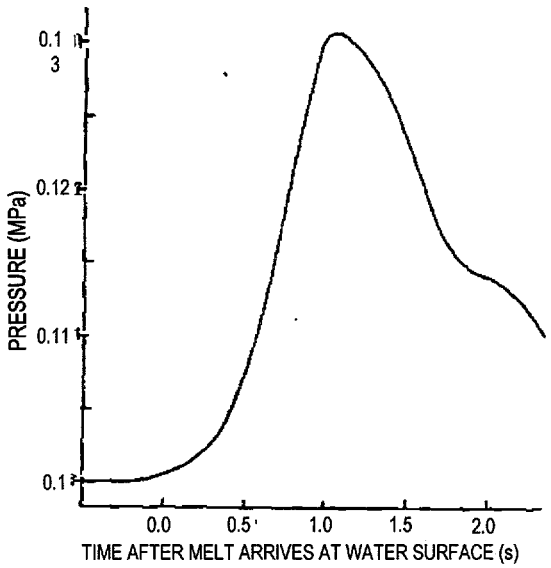

FIGURE 7 THE MEASURED PRESSURE IN THE GAS SPACE FOR EXPERIMENT MIXA-6 (COPIED FROM FLETCHER AND DENHAM, 1995)

peak pressure and the peak steam flow rate would correspond. (The authors are currently in communication with Brian Turland at Winfrith to clarify this point.)

Both of these possibilities are plotted on the pressure-drop/flow-rate curve shown in FIGURE 8. The ordinate of this plot is the product of the steam density (based upon the pressure and assuming the saturation temperature) and the square of the steam volume flow rate. The abscissa is the difference between the pressure and the initial pressure. If the labels of the ordinate of FIGURE 6 and FIGURE 7 are correct then the curve labeled "unmodified" is appropriate. If the ordinate label of FIGURE 7 is incorrect, then the curve labeled "modified" is appropriate.

The initial behavior of both curves is consistent with equation 1. Both curves increase linearly with the product of mass flow rate and volume flow rate. The unmodified curve has a slope of 8106 m^{-4} for the first 0.65 seconds after the melt is released. The "modified curve" has an initial slope of 40816 m^{-4} for the first 0.89 seconds after the melt is released.

Both curves exhibit a behavior inconsistent with equation 1 as the steam flow rate decreases (>1.0 second after the melt is released). Neither curve retraces itself as is expected. The "unmodified curve" shows the pressure drop to increase as the flow rate decreases. The "modified curve" shows the pressure drop nearly invariant during the same period of time. Both curves suggest that something happened to the instrumentation during the experiment. One possibility is that water collected in the flowmeter. Another possibility is that the steam temperature increased. In either case, the data may not be reliable after about 1 second.

In order to maximize the pressurization, the "modified curve"

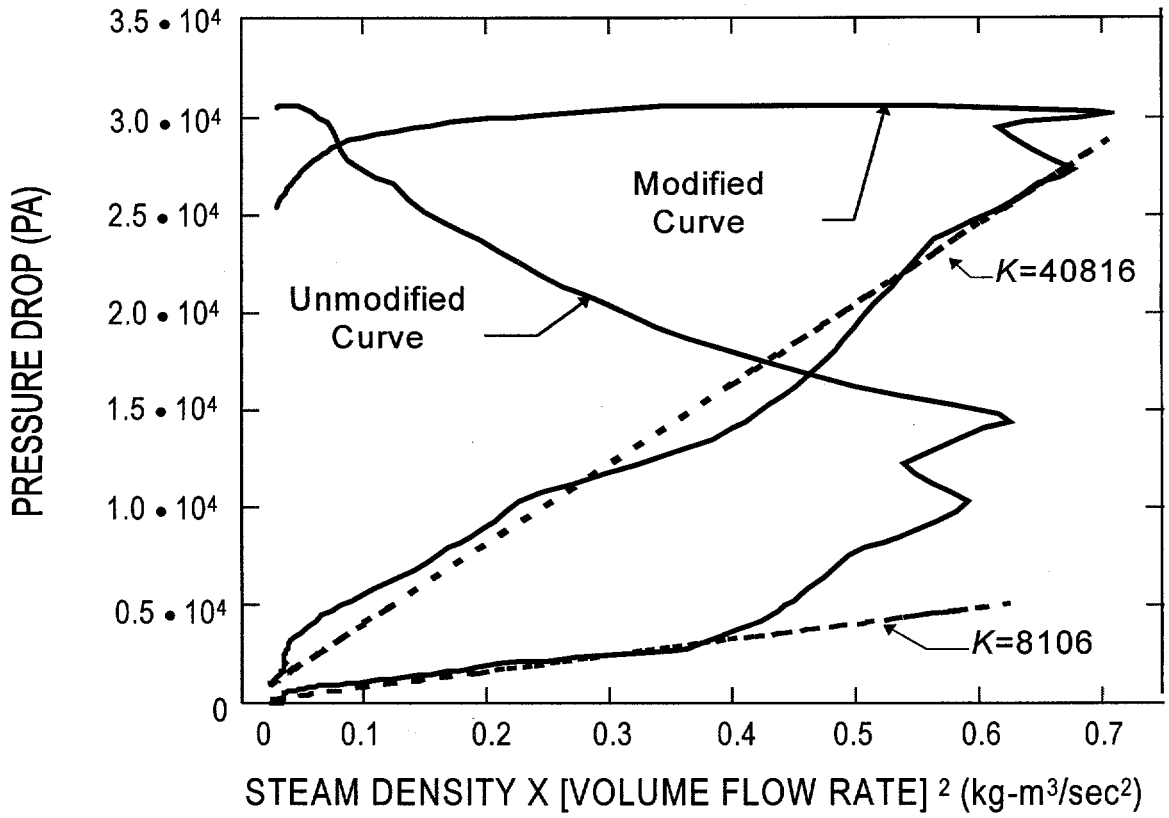

FIGURE 8 PRESSURE-DROP/FLOW RATE CURVE FOR THE MIXA-6 EXPERIMENT

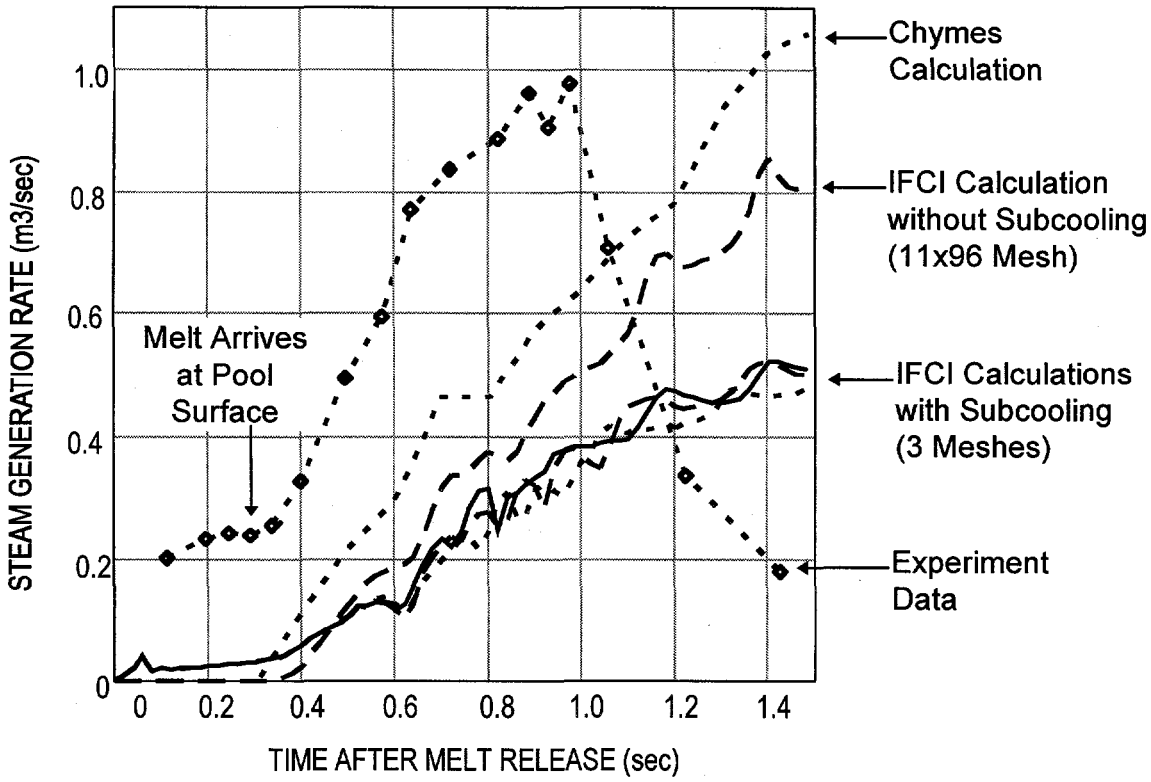

FIGURE 9 STEAM PRODUCTION RATE CALCULATED BY IFCI

was chosen as the basis for calculating the outflow area used in the IFCI simulation. The pressure drop across the outflow boundary condition in IFCI is computed from the equation:

$$\Delta P = \frac{1}{(A_{exit,IFCI})^2} \rho_{steam} (\dot{Q}_{steam})^2 \qquad (2)$$

The exit area used in IFCI ($A_{exit,IFCI}$) is determined by comparing equation 2 to equation 1.

$$A_{exit,IFCI} = \frac{1}{\sqrt{K}} \qquad (3)$$

Using this equation and the "corrected curve", the outflow area to be used in IFCI is 4.9497×10^{-3} m^2.

Comparison of IFCI Predictions with MIXA-6 Measurements

The IFCI predictions for steam generation rate (labeled as "IFCI Calculations with Subcooling") are shown in FIGURE 9 with the data from the MIXA-6 experiment. IFCI clearly underpredicts the steam generation rate by approximately a factor of three. Only minor differences exist between the three meshes (11x36, 11x56, 11x96).

The experiment data suggest one reason for the disparity between measurement and prediction. The data clearly show a significant steam generation rate before the melt hits the water. Since the volume of melt displacing the existing steam is relative small, this initial steam generation measurement can be attributed to only two effects: 1) heating of the steam by the melt falling through the steam, and 2) steam generation in the water due to radiation from the falling melt. An order-of-magnitude analysis shows that the latter of these two possibilities could easily account for the measurement. It is possible that both phenomena contribute to the observation. Neither is modeled in IFCI, which models radiation only within a cell.

Inter-cell radiation may also be necessary for the accurate description of heat transfer during coarse mixing. Currently, the radiative heat transfer between the melt and the water within a cell (E_{rad}) in IFCI is modeled as:

$$E_{rad} = A_{melt} \sigma \left(T_{melt}^{\ 4} - T_{water}^{\ 4} \right) \alpha_{water} \qquad (4)$$

where α_{water} is the water volume fraction in that cell. While this is a reasonable estimate of the radiative heat transfer to the water within the cell, the total radiative loss from the melt should be independent of the cell water volume fraction. Physically, the balance of the radiative loss from the melt would be transferred to the water in adjacent cells. By neglecting this "inter-cell" radiation transport, IFCI underpredicts both the cooling rate of the melt and the consequent steam generation rate.

The case for an inter-cell radiation model is strengthened by an examination of the transmissivity of water. TABLE 2 shows the fraction of energy radiated by the melt that is absorbed by water. The absorbed fraction increases with the path length in the water and decreases with increasing melt temperature. The table

TABLE 2
THE FRACTION OF THERMAL ENERGY ABSORBED AS A FUNCTION OF MELT TEMPERATURE AND PATH-LENGTH (COPIED FROM FLETCHER, 1985)

Path Length (mm)	Fraction of Incident Energy Absorbed		
	T=1000 K	T=2500 K	T=3500 K
1	0.967	0.599	0.343
5	1.	0.707	0.472
10	1.	0.756	0.526
15	1.	0.786	0.560
20	1.	0.806	0.585
25	1.	0.822	0.604
30	1.	0.834	0.620

indicates that approximately 60% of the energy radiated from a 3500 K source across a cell 20 mm wide (the radial cell size used in the IFCI analysis of MIXA-6) would be absorbed by the water in that cell if the cell contained nothing but water. If the cell had only 50% water, then approximately 30% of the radiated energy would be absorbed in that cell with the balance being transmitted into the adjacent cell. These numbers suggest that the transmissivity of water should be included in an inter-cell radiation model in order to correctly predict the local steam generation rate.

Pressurization-induced subcooling also contributed to the low steam generation rate predicted by IFCI. In order to estimate the subcooling effects in the IFCI calculation of MIXA-6, the total heat transferred from the melt to the water was divided by the steam heat of vaporization and the steam density. This quantity is plotted in FIGURE 9 as "IFCI Calculation without Subcooling (11x96 mesh). This curve is less than, but comparable to, the CHYMES (a fuel-coolant interaction code developed by Fletcher and Thyagaraja (1991) at AEA Culham Laboratory) prediction, which assumes saturated conditions. The difference between this curve and the IFCI calculations that include subcooling confirms that subcooling cannot be ignored.

The subcooling models in IFCI are, as yet, not validated. It is clear that inter-cell radiation is important to the successful modeling of the MIXA-6 experiment, and that it will increase the predicted steam generation rate. It is thus concluded that the subcooling models can be evaluated in experiments with high melt temperatures only after a reasonable inter-cell radiation model has been included in the calculation.

CONCLUSIONS

It should be noted at the onset that all of the experiments chosen for this validation exercise are integral in nature and, as such, cannot be used to validate isolated models within the IFCI code. For example, one cannot examine the melt breakup model by comparing the MAGICO experiments to the MIXA experiments. The quantities measured in each experiment are different and are, themselves, the result of many physical processes. These processes include film boiling in two-phase flows, particle drag in two-phase flows, and radiative heat transfer in heterogeneous regions, among others. The differences between the MIXA and MAGICO experiments are due to differences in all of these processes as well as the difference in melt breakup. Using a set of experiments that is progressively complicated is, nonetheless, helpful to the validation process. A critical examination of predicted quantities such as melt front velocity is helped by the absence of particle breakup in the MAGICO experiment

Analysis of the MAGICO-701 experiment demonstrated the importance of meshing in the IFCI prediction. Numerical diffusion in coarse meshes decreases the predicted transit time to the bottom of the container below the experimentally measured times. This might be particularly important in detonation calculations where triggering is induced by contact with the bottom of the container. If the predicted transit time is unphysically small, then the amount of melt involved in coarse mixing at the time of triggering will also be too small. This would affect the predicted strength of the resulting shock.

The analysis of the MIXA-6 experiment suggested the need for the addition of an inter-cell radiation model. Both the data and a "first-principles" analysis indicate this need for a realistic analysis. This is particularly important in light of the need for finer meshes indicated by the MAGICO-701 analysis. As the cell size is reduced, the need for this model increases.

The potential importance of even small amounts of subcooling was also demonstrated in the MIXA-6 analysis. It is, however, impossible to assess the subcooling modeling in IFCI based upon this analysis. The reason is that radiation to the water from the melt competes with the effect of subcooling. It is probable that the addition of an inter-cell radiation transport model in IFCI would increase the predicted steam generation rate. Only after such a model is added can the subcooling model be evaluated by comparison to MIXA data. Evaluation of the subcooling model using an experiment with a low-temperature melt would also be advisable, since this would strongly reduce the radiation heat transfer to the water.

In summary, the validation exercises conducted so far have been highly productive. Detailed examination of the experimental data and comparison to IFCI predictions has identified important modeling improvements that would significantly enhance IFCI capabilities. In addition, the work has enabled important improvements in the numerics of the code to be made, and pointed out other areas where further work on code numerics would be useful.

REFERENCES

Davis, F. J., and Young, M. F., Integrated Fuel-Coolant Interaction (IFCI 6.0) Code, NUREG/CR-6211, SAND94-0406, Sandia National Laboratories, Albuquerque (1994).

Denham, M. K., Tyler, A. P., and Fletcher, D. F., "Experiments on the Mixing of Molten Uranium Dioxide with Water and Initial Comparisons with Chymes Code Calculations," Proceedings of the Fifth International Topical Meeting on Reactor Thermal Hydraulics (NURETH-5), Vol VI, Salt Lake City, Ut, USA (September 21-24, 1992).

Fletcher, D. F., Assessment and Development of the Bankoff and Han Coarse Mixing Model, CLM-R252, Culham Laboratory, Abingdon (1985)

Fletcher, D. F., and Thyagaraja, A., "The CHYMES Coarse Mixing Model", Prog. Nucl. Energy, 26, 31-61 (1991).

Fletcher, D. F., and Denham, M. K., "Validation of the Chymes Mixing Model," Nuclear Engineering and Design, 155 (1995).

Theofanous, T. G, Yuen, W. W., Angelini, S., Chen, X., Amarasooriya, W. H., and Medhekar, S., Steam Explosions: Fundamentals and Energetic Behavior, NUREG/CR-5960, Department of Chemical and Nuclear Engineering, Center for Risk Studies and Safety, University of California at Santa Barbara (1994).

Young, M. F., "Application of the Integrated Fuel-Coolant Interaction Code to a FITS-Type Pouring Mode Experiment," Dynamics of Detonations and Explosions: Explosion Phenomena; Progress in Astronautics and Aeronautics, 134 (1991).

NOMENCLATURE

A area (m^2)
E heat transfer (W)
k pressure loss coefficient (dimensionless)
K exit pressure loss coefficient (m^{-4})
P pressure (MPa)
Q volume flow rate (m^3/sec)
T temperature (K)

α volume fraction (dimensionless)
ρ density (kg/m^3)
σ Stefan-Boltzmann constant ($5.7 \bullet 10^{-8}$ $W/m^2\text{-}K^4$)